Hybrid Visual Servo Control for Point-to-Point Localization of an Autonomous Wheeled Mobile Robot

You-Fu Chiang, Yen-Heng Liu, Chun-Ta Chen*

***Abstract*—Position-based visual servo (PBVS) control and image-based visual servo (IBVS) control have been the viable approaches to control of autonomous mobile robots and manipulators in an eye-in-hand manner. However, PBVS suffers from the sensitivity to model for position calculation, and IBVS is limited to the field of view (FOV) covered. In this paper, a hybrid visual servo control (HVSC) integrating PBVS and IBVS was proposed for tradeoff of both performances. To achieve the visual servo control, a fixed depth camera is mounted to an autonomous wheeled mobile robot (WMR) for visual feedback information. Point-to-point localization tasks were executed for the WMR. Experimental results demonstrate the feasibility and effectiveness of the proposed hybrid visual feedback schemes.**

I. INTRODUCTION

WMRs possess a simple structure, flexible navigation, and low cost [1], and have been widely applied to in real environment such as industry, home and military, etc. Recently, to improve the autonomy of WMR, the visual servo control of WMR has become an active research topic in the control and robotics communities [2].

The visual servo control for WMR is designed by integrating feedback information from vision sensors or cameras into the control loop. Cameras have small size and high resolution, and can provide abundant information about the environment. For applications of autonomous WMR, the eye-in-hand configuration is always taken as the installation manner of camera, where the camera is mounted on the WMR body. In addition, according to the error signal, the visual servo controls are classified as PBVS, IBVS and HVSC [3, 4].

In the PBVS algorithm, a 3D model of environment and camera parameters are required. The reverent 3D parameters are computed through the pose of the camera within a reference frame. The absolute or relative positions of WMR with respect to target objects can thus be determined using the visual 3D parameter information. The controllers are then designed based on the position errors such that the WMR can navigate to a desired point, or execute a target searching like the leader–follower action. Sharma et al. [5] implemented PBVS for a mobile robot using gradient descent-based estimation for online parameter estimation for a desired position and orientation. The proposed adaptive technique achieved both estimation and control tasks. Chen et al. [6] used PBVS for robot pose estimation to avoid obstacles. The work comprises of feature extraction for PBVS and collision avoidance within the task space. The PBVS control is used for the robot motion. Deng et al. [7] summarized the various implementations of the PBVS methods according to the dynamic performance in the Cartesian and image spaces. The results show that straight line Cartesian trajectories can be guaranteed in the desired static end-effector frame, but the image trajectories are not controlled and may leave the FOV of camera. However, in PBVS, exact knowledge of intrinsic parameters of camera is required for control performance. Even very small errors in the camera calibration may largely affect the control accuracy of robots.

IBVS directly uses image features that are converted from pixels-expressed image by the camera system to design controllers. Visual features are first extracted from the image space. The errors are computed from points or vectors by the visual features. Aliakbarpour et al. [8] presented the radial model with a non-central catadioptric camera to allow effective IBVS of a mobile robot. The new visual features can control the motion of a mobile robot moving on plane. Zhang et al. [9] took advantage of the image features in the IBVS to achieve a direct and fast motion planning solution, in which surplus features and image-based constraints are incorporated. Shi et al. [10] presented an adaptive control method in IBVS using RL for WMR. The real-time adjustment of the image Jacobian matrix by fuzzy state coding accelerates learning at the training phase. Although the IBVS schemes are robust to the calibration errors in camera, large calibration errors may cause the closed-loop system to be instable [11]. As a result, an advanced control design is required for stability. Moreover, the IBVS by the fixed camera on WMR is limited to a field of view. That is, the target may always move out of the field of view as the WMR turns, and the IBVS controller will fail to control the WMR.

HVSC improves PBVS and IBVS without camera calibration or a target model, and may perform better stability [12]. HVSC combines the Cartesian and image measurements for error functions [13]. The rotation and the scaled translation of camera between the current and desired views of an object are estimated as the displacement of camera. Lots et al. [14] presented hybrid visual servoing for station-keeping an underwater vehicle. The restrictive controllability of the vehicle was considered because of the thruster's configuration. However, the proposed HVSC are susceptible to image noise. Li and Xiong [15] proposed an HVS-based control method for a mobile manipulation robot. The HVS control was developed using the whole Jacobian matrix combined with position and visual image information. However, a Kalman filter was introduced to correct the positions and orientations of the end of the manipulator to avoid the observed position error. Sharma et al. [16] presented a hybrid approach to robust servoing for WMR. The heading restoration method was designed based on an optical flow to deal with the visual marker disappearing from the FOV of the camera. However,

the arduous reinforcement learning was used to solve this visibility problem. The efficacy of proposed scheme was proven by simulation and experimental results.

Although HVSC has been proposed for the localization and navigation control of WMR, almost the HVSC simultaneously applied the PBVS and IBVS to formulate the vision Jacobian to design the feedback control. In this paper, the HVSC alternatively integrating PBVS and IBVS was proposed for tradeoff to implement the point-to-point localization of WMR.

II. Mobile Robot Model with Nonholonomic Constraint

A. Wheel mobile robot building

The mechanical structure of WMR is shown in Fig. 1. The mobile robot is driven by a differential drive system, which uses the difference speed between left and right wheel speed to execute longitudinal and lateral movements. The mobile robot consists of driving wheels and driven wheels, and the PC sends instructions to the motor drivers for driving wheels (ELVDR-K020CQ). As shown in Fig. 2, the hardware design of this research includes two DC brushless motors (BL60L, Ø54mm, 120W), each motor is mounted with a planetary gear reduction mechanism (2GB23M). The Hall sensor uses a magnetic field to convert the voltage, and calculates the left and right wheel speeds through external interruption of timer integration and negative edge triggering. The spatial coordinate information of the target extracted by the depth camera (Intel realsense2 D435i) is used to realize the visual servo feedback position control. Finally, the control algorithms and measurements were developed in Python.

B. Kinematics Model

The kinematics of the simplified WMR with differential drives is shown in Fig. 3, in which the inertial frame O_XY is fixed to the ground. The body-fixed frame C_xy is mounted to the WMR with the origin C being assigned to the center of mass (*CM*), where the x axis is defined as the heading direction of WMR, and the y axis is directed to the side direction. It is assumed that the kinematics of WMR satisfies the non-holonomic constraint, i.e. the left and right driving wheels cannot slide sideways, and thus the side velocity $v_y = \dot{Y}\cos\theta - \dot{X}\sin\theta$ is zero. Moreover, the heading velocity v_c of WMR, being the velocity of *CM* along the x direction, can be expressed by the average of the right/left wheel velocities as

$$v_c = v_x = (v_{R,x} + v_{L,x})/2 = r(\omega_R + \omega_L)/2 \tag{1}$$

in which r is wheel radius, ω_R, ω_L are the respective rotational speed of the right/left wheel.

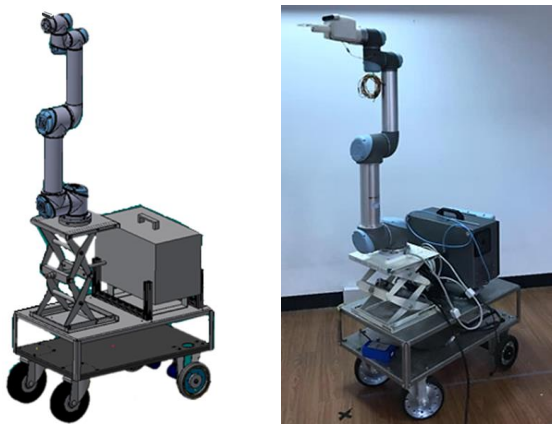

(a) (b)

Figure 1. (a) Proposed WMR design. (b) Autonomous system building.

Figure 2. Control circuit and peripherals.

The yaw rate of WMR is resulted from the velocity difference between the right and left wheels, and can be written as

$$\omega_c = r(\omega_R - \omega_L)/b \tag{2}$$

in which b is the width of WMR. Eqs.(1)(2) implies that the right/left wheel speeds dominate the heading velocity and yaw rate of WMR.

In addition, the general velocities in the inertial frame shown in Fig. 3 are related to the heading velocity and yaw rate, and also to the rotation speeds of the two wheels of the WMR as

$$\dot{\boldsymbol{q}} = [\dot{X} \quad \dot{Y} \quad \dot{\theta}_z]^T = [v_c\cos\theta \quad v_c\sin\theta \quad \omega_c]^T = \boldsymbol{J\omega} \tag{3}$$

in which $\boldsymbol{J}=\begin{bmatrix} (r\cos\theta)/2 & (r\cos\theta)/2 \\ (r\sin\theta)/2 & (r\sin\theta)/2 \\ r/b & -r/b \end{bmatrix}$ means the Jacobian matrix, $\boldsymbol{\omega} = [\omega_R \quad \omega_L]^T$. The kinematic equation implies a relation of the state of WMR to the heading velocity and heading angles, and hence the control on the wheel velocities of WMR can localize the global position.

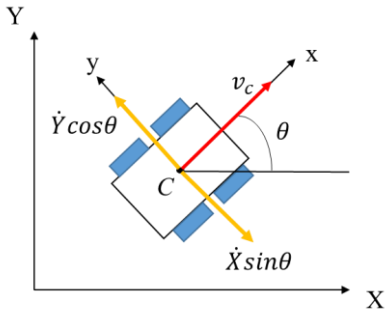

Figure 3. Kinematics of WMR and defined coordinate systems.

III. Visual Servo Control Design

The WMR aims to search for the target, and then will be driven to the desired location for the ensuing actions. Therefore, a machine vision must be installed for visual servo control to realize the point-to-point localization. As such, this section will present the visual servo control designs combing with a cascade inner-loop control.

A. PBVS Cascade Control

In the PBVS control method, the target is identified by the color depth camera with respect to the global frame. The image-expressed information is first processed, and then converted to the position of the camera plane relative to the WMR in the inertial frame. As shown in Fig. 4, it is supposed that the position of the WMR is (x_c, y_c), the coordinate of the desired target point P is (x_p, y_p), the distance between the desired target and the WMR is defined as the distance error d_e, and can be expressed as

$$d_e = \sqrt{\left(x_p - x_c\right)^2 + \left(y_p - y_c\right)^2} \tag{4}$$

The desired final heading direction β can be specified. If the final heading direction is not specified, the direction of the position of the desired target position P with respect to the initial position C will be designated as the desired posture. Using the arctangent trigonometric function, the final posture is determined as

$$\beta = atan(\frac{y_p - y_c}{x_p - x_c}) \tag{5}$$

The heading direction error is then defined as the difference of the final heading angle and the initial heading angle as $\theta_e = \beta - \theta$. These two polar coordinate values serve as the visual feedback for control of the WMR. And the reference heading velocity v_c and yaw rate ω_c are synthesized as the control commands based on the Lyapunov stability theory.

If a Lyapunov candidate function is chosen as [17]

$$V = \frac{1}{2}\lambda {d_e}^2 + \frac{1}{2}\left({\theta_e}^2 + h\beta^2\right) \tag{6}$$

which is positive and differentiable. Taking derivative on V and combining with Eqs. (3-5) lead to

$$\dot{V} = \lambda d_e(-v_c cos\theta_e) + (\theta_e\left(\frac{v_c sin\theta_e}{d_e} - \omega_c\right) + \frac{h\beta v_c sin\theta_e}{d_e}) \tag{7}$$

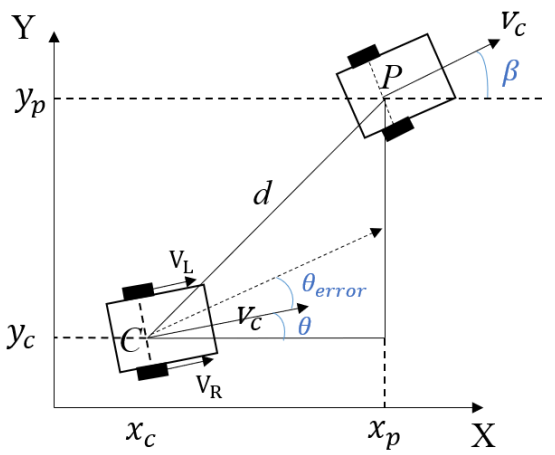

Figure 4. Positions and heading directions of WMR.

The reference commands are assigned as

$$v_c = (\alpha\, cos\theta_e)\, d_e \tag{8}$$

$$\omega_c = k\theta_e + \alpha\frac{cos(\theta_e)\, sin(\theta_e)}{\theta_e}(\theta_e + h\beta) \tag{9}$$

the derivative of the Lyapunov function becomes

$$\dot{V} = -\alpha\lambda {d_e}^2\, cos^2(\theta_e) - k{\theta_e}^2 \leq 0 \tag{10}$$

The asymptotically stability of the system is thus guaranteed

Because in the kinematic model the rotational speeds of wheels are the control inputs to the WMR, the reference commands v_c, ω_c are further converted to the desired rotational speeds of wheels. From the simultaneous Eqs. (1)(2), the rotational speeds of the right/left wheel are determined as

$$\boldsymbol{\omega} = [(2v_c + B\omega_c)/2r \quad (2v_c - B\omega_c)/2r]^T \tag{11}$$

Furthermore, both wheels of the WMR are driven by motors. The control inputs $\boldsymbol{u}$ to the corresponding motors must ensure that the actual rotational speeds of wheels can track the desired rotational speeds. In this regard, the PI controller is employed for the feedback control of the wheels, in which the actual rotational speeds of wheels are measured by the Hall sensors that are connected to electric motors.

The proposed PBVS cascade controller is composed of two controllers connected in series to achieve the point-to-point localization. The cascade control structure, consisting of a heading direction error controller and a distance error controller, is proposed for the high level to drive the WMR to the target point [18]. As shown in Fig. 5, in the outer loop the reference heading velocity v_c and yaw rate ω_c are synthesized as the control commands by the position error feedback. The inner loop is a PI controller for the wheel control of WMR. It is noted that the position of the WMR is calculated by the kinematic model. Additionally, the dead reckoning method that is called the odometry was employed to calculate the relative state with respect to the initial posture based on data from incremental wheel encoders. The advantage of the cascade structure is that the inner loop directly regulates the distance and heading direction errors under external disturbances. That ensures a stable localization. To reduce the localization error, the position of target point with respect to

the WMR is modified through the vision feedback every execution time until the target is out of FOV.

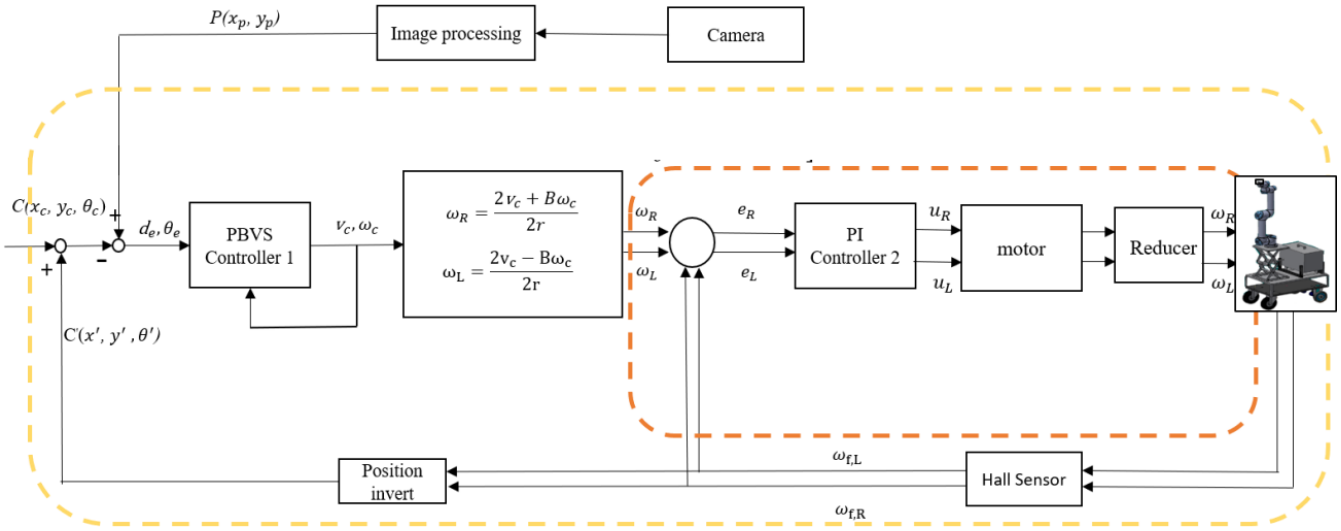

Figure 5. PBVS-based cascade control.

B. IBVS Fuzzy Cascade Control

IBVS is based on the images captured from a camera to acquire the characteristics information of targets. Needing not a conversion from the 2D pixel coordinates to the 3D space coordinates, IBVS is designed based on the pixel errors on the image plane.

Supposed that a target appears in the image plane with the pixel coordinate $\boldsymbol{u_p}$=(u_p v_p). The pixel coordinates of principal point is $\boldsymbol{u_c}$ =(u_c v_c). When the WMR moves, the abscissa u of the target in the image plane is considered for localization control since the ordinate v of the image plane varies with u. As a consequence, the depth error is further considered for the control design of the differential driven WMR. The errors of the abscissa u and the depth value Z are respectively defined as

$$\boldsymbol{e} = [e_u \quad e_d]^T = [u_p - u_c \quad z_p - z_c]^T, \tag{12}$$

These two error values from the image taken by the depth camera will be used for the determination of reference heading velocity v_c and yaw rate ω_c. In this study, the fuzzy theory is applied to synthesize the reference commands.

The fuzzy function *FUZZY* maps two linguistic input variables e_u, and e_d to linguistic output based on the Mamdani inferred rules without a detailed input-output model. The fuzzy rules are shown in Table 1, in which seven fuzzy rules for e_u input are NB (Negative Big), NM (Negative Medium), NS (Negative Small), ZE (Zero), PS (Positive Small), PM (Positive Medium) and PB (Positive Big), and four fuzzy rules for e_d are defined as ZE, PS, PM and PB. The fuzzy logic IF-THEN rule base determines the input-output relationships in the fuzzy inference system which are typically used in the fuzzy inference system as shown in Table I, and is expressed as $R^{(ij)}$ ::IF e_u is A_1^i and e_d is A_2^j THEN $FSMC_{ij}$ is B^{ij}, i=1,…,4; j=1,…7, in which A_1^i, and A_2^j are the input fuzzy sets; B^{ij} is the output fuzzy set. The normalized membership functions of input and output linguistic variables are chosen as in Fig. 6. Correlation-minimum inference with centroid defuzzification method is used for the fuzzy implications, and thus the reference heading velocity v_c and yaw rate ω_c can be adjusted adaptively according to the pixel error e_u of abscissa and the depth error e_d.

Identical to the PBVS cascade control, the reference commands v_c , ω_c are converted to the desired rotational speeds of wheels, and then the control inputs $\boldsymbol{u}$ to the corresponding motors are designed by the PI controller with the feedback of rotational speed errors between the desired rotational speed and the actual rotational speeds of wheels. The proposed IBVS fuzzy cascade control is shown in Fig. 7.

TABLE I. FUZZY RULES FOR IBVS

e_u \ e_d	ZE	PS	PM	PB
NB	PS	PM	PM	PB
NM	PS	PS	PM	PB
NS	ZE	PS	PM	PM
ZE	ZE	PS	PM	PM
PS	ZE	PS	PM	PM
PM	PS	PS	PM	PB
PB	PS	PM	PM	PB

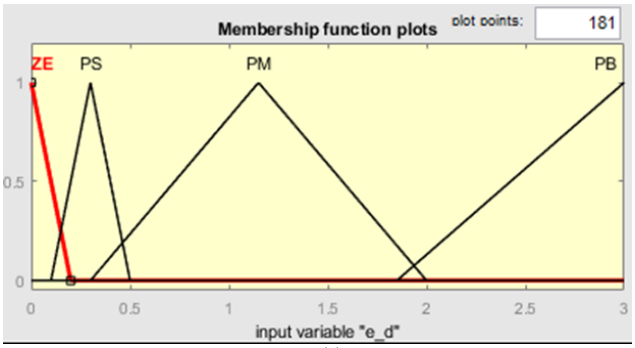

(a)

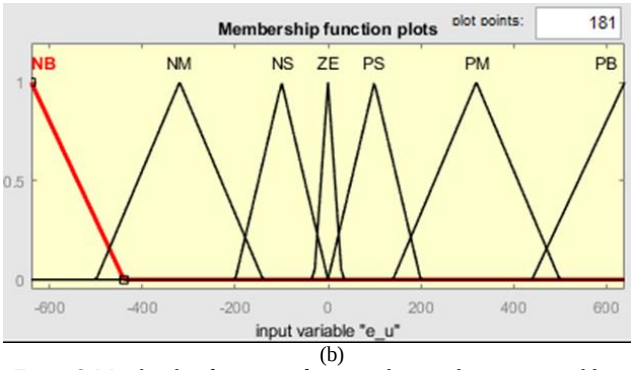

(b)

Figure 6. Membership functions of input and output linguistic variables.

C. Hybrid Visual Servo Control

As mentioned above, PBVS cascade controller makes use of the depth stereo camera to identify the target, and then the associated position is calculated by converting the desired point in image frame to the space coordinates. However, the conversion may result in the uncertain error because of the intrinsic and external camera parameters. Also, in the process of traveling, the errors of WMR's position will cause serious localization deviation due to unexpected external disturbance such as friction and slip. The errors of position even are accumulated more and more with the traveling distance. and thus the required calculation loading is comparatively lessened. Moreover, the target information is constantly returned for feedback control while traveling, it has higher localization accuracy than PBVS under the identical disturbances. But the pixel-based control may cause the WMR to generate a larger response in space. The main drawback of IBVS by the fixed camera is the limited field of view. When the WMR turns, the target is always out of the field of view, and the IBVS will fail to control the WMR. Therefore, a HVSC integrating PBVS and IBVS was proposed for tradeoff.

The HVSC is presented in Fig. 8 for visual servo control. IBVS is first applied to execute the point-to-point localization of WMR due to the better control accuracy. Afterwards, PBVS will continue the ensuing navigation to achieve the remaining localization task according to switching conditions. Based on several tests, in this study, one of the switching conditions is prescribed as $e_u \leq 5$, $e_d \leq 0.2$. The other switching condition is that the target is detected to be soon beyond the field of view. The shorten distance to the target may reduce the accumulated localization error for PBVS, and fasten the localization speed. The tradeoff by HVSC improves the point-to-point localization accuracy on WMR. It is noted that when the PBVS is first applied in HVSC, if the target moves out of the FOV, the PBVS can still achieve the localization by the final recorded position of the target. But IBVS can't implement a localization without the target on the FOV of the fixed camera. As such, the HVSC will be equivalent to PBVS if PBVS is first applied.

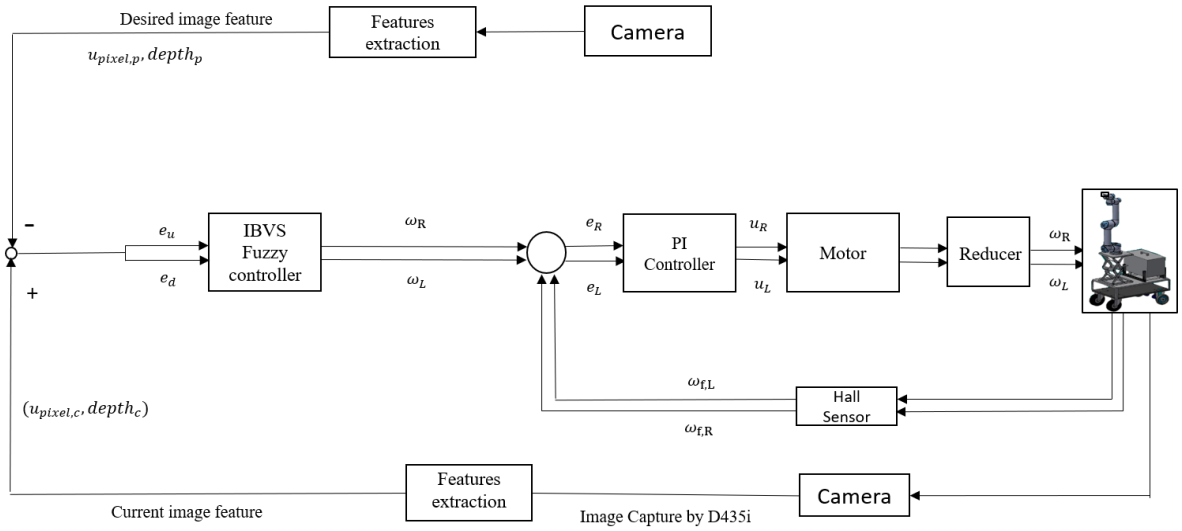

Figure 7. IBVS fuzzy cascade control.

IBVS takes advantage of pixel coordinates in image plane for feedback control without conversion to space coordinates,

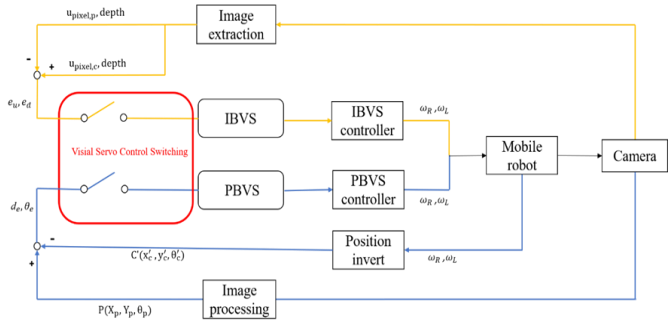

Figure 8. HVSC structure.

IV. Experiments and Results

As shown in Fig. 9, the proposed visual servo control algorithms were demonstrated by our built WMR with a depth camera being mounted to the end-effector. The experimental field is an indoor room paved with the wooden floor. The initial heading direction is θ=0. A cherry tomato located in front of the WMR is referred as the target whose position with respect to the WMR is (3.26, 1.267) m. This test field may simulate a greenhouse, and the point-to-point localization experiments may simulate a search for mature crops by the autonomous motion of WMR.

In addition, the Ultra-Wide-Band (UWB) was used to measure and record the trajectory of WMR. In the tests, four anchors are put around the corners of the room, and a tag on the WMR. The distance from the four anchors can be measured by the tag according to a certain frequency. The position of WMR was thus calculated, and hence the trajectories of WMR can be recorded.

The required parameters for the proposed controllers are taken the followings: in the PBVS cascade control, $\alpha = 0.1$, $k = 0.85$, h=0.015. The switching conditions for HVSC are e_d =0.2m, e_u =5pixels. And $K_p = 0.8$, $K_I = 0.3$ for PI controller.

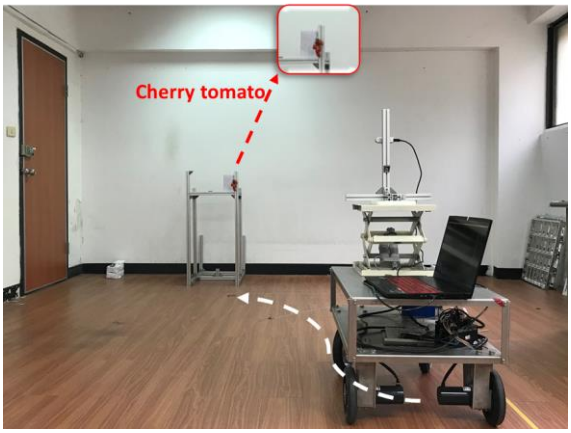

Figure 9. Indoor positioning experiment with UWB.

A. Final Posture β Is Not Specified

In the experiment for non-specified β, the final position of WMR is assigned as the distance error e_d =0.2m from the target. The three visual feedback controllers were applied to implement the point-to-point localization of the WMR. The trajectories to the final stopping position are shown in Fig. 10. Because the target is always inside the field of view of the WMR in the experiment, the trajectories for IBVS and HVSC are very close.

The error comparisons of final posture for the proposed visual feedback controllers are shown in Fig. 11, in which the distance from the final point to the target was measured by the laser displacement measurement. It is seen that the error by PBVS are larger than the other algorithms due to the cumulative errors while moving as well as the calculated position from the kinematic model. However, as shown in Table II, PBVS has a faster finishing time 8.68 sec. for the point-to-point localization since the IBVS and HVSC must frequently capture the image to serve as the feedback information such that the finishing time almost doubles than PBVS.

The point-to-point motion of the WMR by HVSC is presented in Fig. 12. It can be seen the proposed visual servo control can smoothly drive the WMR to the desired position.

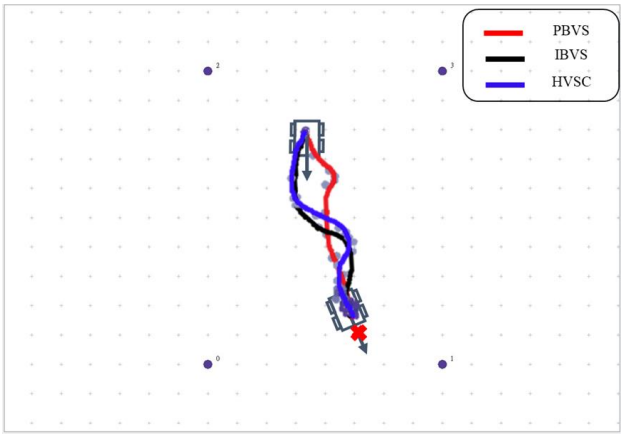

Figure 10. Trajectories of WMR by PBVS, IBVS and HVSC for non-specified β.

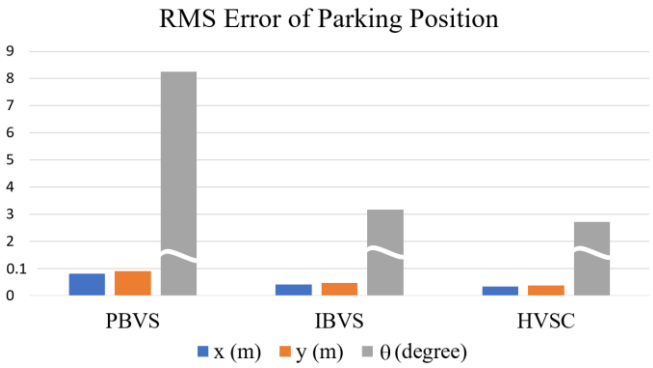

Figure 11 Error comparisons of PBVS, IBVS and HVSC for non-specified β.

B. Final Posture $\beta = 90^{\circ}$

In the experiment, the final posture of WMR is assigned to be β=90°, and it is implied the target will be out of the field of view after turning during the motion. Therefore, as shown in Fig. 13 for the trajectories, IBVS make the WMR fail to move to the desired destination. The proposed HVSC combining IBVS and PBVS drive the WMR first using IBVS fuzzy cascade control to the target position. Before the target exceeds the field of view of the camera, the hybrid visual servo

controller was switched to the PBVS cascade controller to continue the ensuing movement. The shorten distance from the target can reduce the error accumulation of the calculated position. The final localization error is 0.03 ± 0.01m by the laser displacement measurement, and the final heading direction error is less than 5° as shown in Fig. 14 for the localization error comparisons in PBVS, IBVS and HVSC. Table III presents the finishing time for the point-to-point localization by the three visual servo controllers.

TABLE II. FINISHING TIME FOR NON-SPECIFIED β

Method / Time	PBVS	IBVS	HVSC
Time(s)	8.68	16.23	15.78

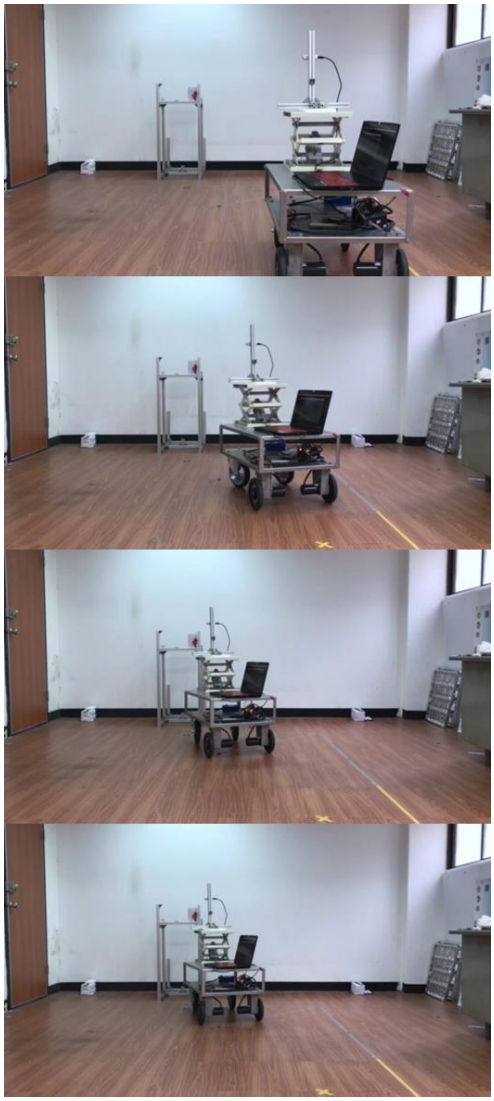

Figure 12. Point-to-point motion by HVSC for non-specified β.

Fig. 15 shows the point-to-point localization motion by HVSC for $\beta = 90^\circ$. The marked switching point means that the controller of the WMR is switched from the IBVS to PBVS at the position due to the disappearing target soon from the field of view. The results demonstrate the successful point-to-point localization by the proposed HVSC.

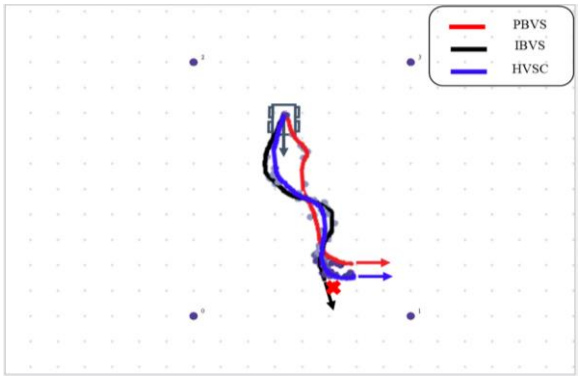

Figure 13. Trajectories of WMR by PBVS, IBVS and HVSC for β=90°.

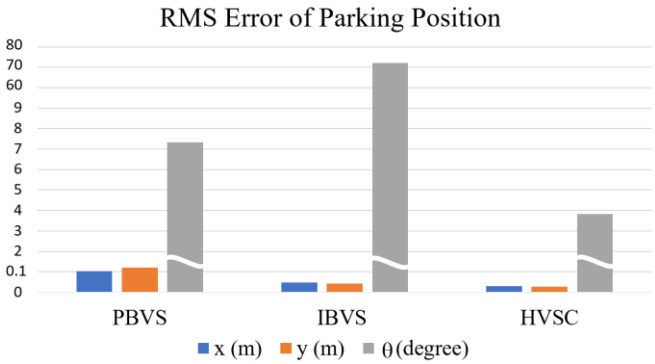

Figure 14. Error comparison of PBVS, IBVS and HVSC for β=90°.

C. *Final Posture* $\beta = 0^\circ$

In the experiment, the WMR was assigned to stop beside the target with the final heading direction $\beta = 0^\circ$. The trajectories of WMR by PBVS, IBVS and HVSC are presented in Fig. 16, in which the point-to-point localization task failed by IBVS because the fixed eye-in-hand characteristics always have the camera capture no the target while turning. From the Fig. 17 for the localization error comparisons, the HVSC has superior point-to-point localization performance. However, HVSC still spent more time 24.53 sec to finish the task as depicted in Table IV.

The successful point-to-point localization motion by HVSC is presented in Fig. 18, in which the switching condition at the switching point is based on the e_u=5pixels.

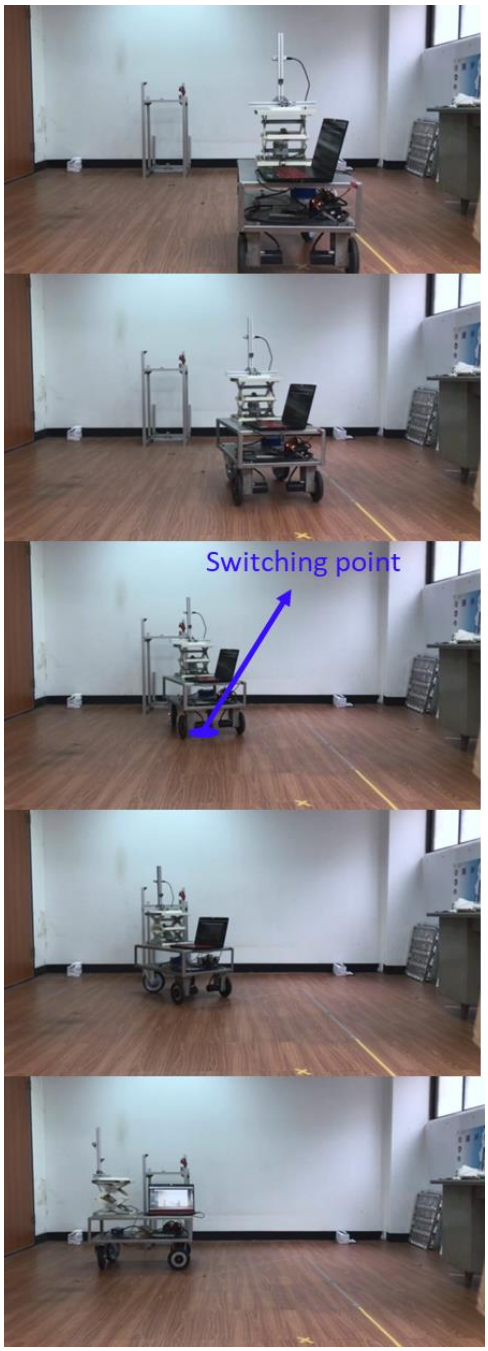

Figure 15. Point-to-point motion by HVSC for β=90˚.

TABLE III. FINISHING TIME FOR β=90˚

Time \ method	PBVS	IBVS	HVSC
Time(s)	12.77	15.94	18.86

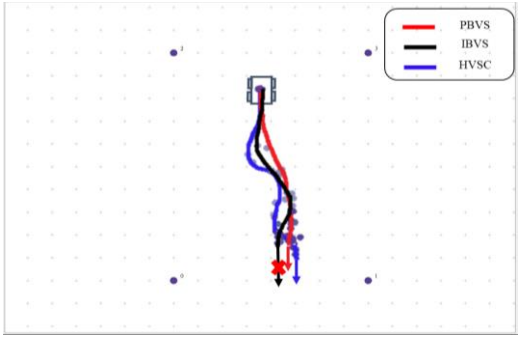

Figure 16. Trajectories of WMR by PBVS, IBVS and HVSC for β=0˚..

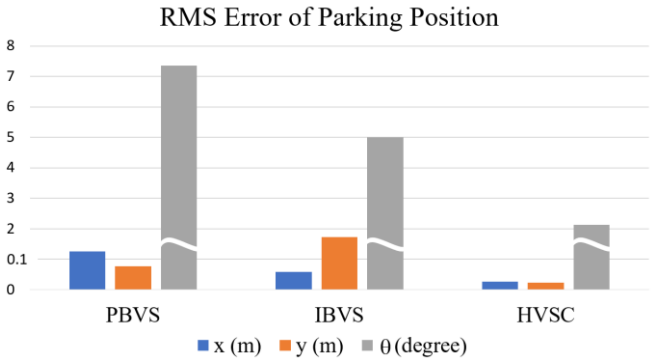

Figure 17. Error comparisons of PBVS, IBVS and HVSC for β=0˚

TABLE IV. FINISHING TIME FOR β=0˚

Time \ Method	PBVS	IBVS	HVSC
Time(s)	18.97	15.31	24.53

V. CONCLUSIONS

This paper concludes with the realization of a hybrid visual servo controller for a proposed WMR on point-to-point localization. To perform smooth and accurate localization tasks, the IBVS fuzzy cascade control is first used to implement the tasks. If the target can't be captured due to a turning, the controller is switched to the PBVS cascade control to continue the following movement. The point-to-point localization experiments for different final heading directions by our built WMR show that HVSC gives the superior performance in localization accuracy over pure IBVS and PBVS. Besides, investigations on finishing time give a faster travelling but a poor localization precision.

In the future, the visual servo algorithm will be further studied in agricultural fields for practical applications. In addition, a manipulator will be installed on the WMR to perform crop harvesting. It is expected that the efficacy of such an autonomous WMR system can be fully assessed in providing agricultural applications.

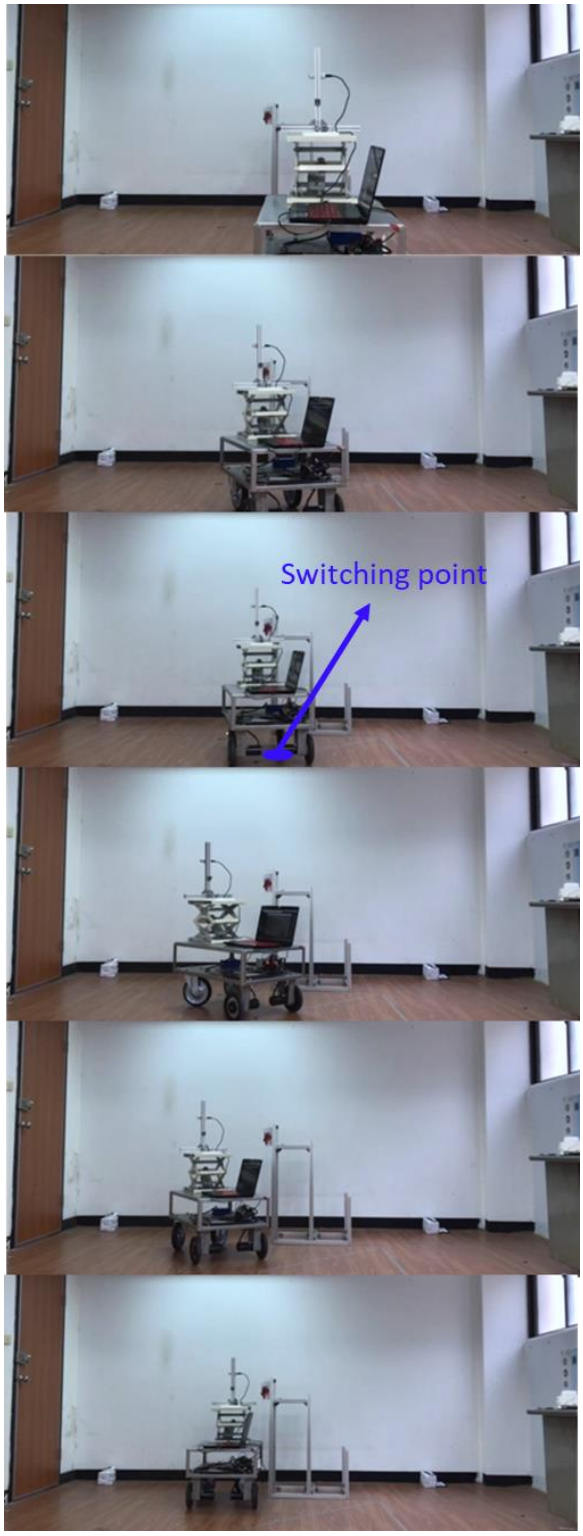

Figure 18. Point-to-point motion by HVSC for β=0˚.

ACKNOWLEDGMENT

This work was supported by the Ministry of Science and Technology of Taiwan under the Grant No. MOST 108-2321-B-027-001 and MOST 108-2221-E-003-024 -MY3.

REFERENCES

[1] A. Stefek, T.V. Pham, V. Krivanek and K. L. Pham, "Energy comparison of controllers used for a differential drive wheeled mobile robot," IEEE Access, vol. 8, pp. 170915-170927, 2020.

[2] H. Shi, M. Xu and K.S. Hwang, "A fuzzy adaptive approach to decoupled visual servoing for a wheeled mobile robot," IEEE Transactions on Fuzzy Systems, vol. 28, no. 12, pp. 3229-3243, 2020.

[3] X. Liang, H. Wang, Y.H. Liu, W. Chen and Z. Jing, "Image-based position control of mobile robots with a completely unknown fixed camera," IEEE Transactions on Automatic Control, vol. 63, no. 9, pp. 3016-3023, 2018.

[4] N. Gans, S. Hutchinson, P. Corke, "Performance tests for visual servo control systems with application to partitioned approaches to visual servo control," International Journal Robot Research, vol. 22, pp. 955–981, 2003.

[5] R. Sharma, S. Shukla, L. Behera and V. Subramanian, "Position-based visual servoing of a mobile robot with an automatic extrinsic calibration scheme," Robotica, 38(5), pp. 831–844, 2020.

[6] H. Shi, J. Chen, W. Pan, K. Hwang and Y. Cho, "Collision avoidance for redundant robots in position-based visual servoing," IEEE Systems Journal, 13(3), pp. 3479–3489, 2019.

[7] L. DENG, W.J, WILSON, F. JANABI-SHARIFI, "Dynamic performance of the position-based visual servoing method in the cartesian and image spaces," In: Proceedings 2003 IEEE/RSJ International Conference on Intelligent Robots and Systems (IROS 2003), pp. 510-515, 2003.

[8] H. Aliakbarpour, O. Tahri, and H. Araujo, "Visual servoing of mobile robots using non-central catadioptric cameras," Robotics and Autonomous Systems, vol. 62, pp. 1613–1622, 2014.

[9] H. Zhang and J. P. Ostrowski, "Visual motion planning for mobile robots," IEEE Transactions on Robotics and Automation, vol. 18, no. 2, pp. 199–208, 2002.

[10] H. Shi, H. Wu, C. Xu, J. Zhu, M. Hwang and K.S. Hwang, "Adaptive image-based visual servoing using reinforcement learning with fuzzy state coding," IEEE Transactions on Fuzzy Systems, vol. 28, no. 12, pp. 3244-3255, 2020.

[11] A. Singh, V. Kalaichelvi, R. Karthikeyan," A survey on vision guided robotic systems with intelligent control strategies for autonomous tasks," Cogent Engineering, 9(1), pp.1-44, 2022.

[12] E. Malis, F. Chaumette, S. Boudet, "2 1/2 d visual servoing," IEEE Transactions on Robotics and Automation, 15(2), pp. 238–250, 1999.

[13] Z. Machkour, D. Ortiz-Arroyo, P. Durdevic, "Classical and deep learning based visual servoing systems: a survey on state of the art," Journal of Intelligent and Robotic Systems, 104(11), pp.1-27, 2022.

[14] J.F. Lots, D. Lane, E. Trucco, "Application of 2 1/2 d visual servoing to underwater vehicle station-keeping," In: OCEANS 2000 MTS/IEEE Conference and Exhibition. Conference Proceedings, vol. 2, pp. 1257–1264, 2000.

[15] W. Li, R. Xiong, "A hybrid visual servo control method for simultaneously controlling a nonholonomic mobile and a manipulator," Frontiers of Information Technology & Electronic Engineering, 22(2), pp. 141-154, 2021.

[16] R. S. Sharma, R. R. Nair, P. Agrawal, L. Behera and V. K. Subramanian, "Robust Hybrid Visual Servoing Using Reinforcement Learning and Finite-Time Adaptive FOSMC," IEEE Systems Journal, vol. 13, no. 3, pp. 3467-3478, 2019.

[17] M. Aicardi, G. Casalino, A. Bicchi and A. Balestrino, "Closed loop steering of unicycle like vehicles via Lyapunov techniques," IEEE Robotics and Automation Magazine, vol. 2, no. 1, pp. 27-35, 1995.

[18] F. Dong, W. Heinemann, R. Kasper. "Development of a row guidance system for an autonomous robot for white asparagus harvesting", Computers and Electronics in Agriculture, vol. 79, pp. 216-225, 2011.